

## THE PHYSICAL CONDITIONS IN A POLAR CORONAL HOLE AND NEARBY REGIONS FROM NORIKURA AND *SOHO* OBSERVATIONS

K. P. RAJU,<sup>1,2</sup> T. SAKURAI,<sup>1</sup> K. ICHIMOTO,<sup>1</sup> AND JAGDEV SINGH<sup>2</sup>

Received 2000 March 12; accepted 2000 June 6

### ABSTRACT

The distribution of emission-line intensities, Doppler velocities, and line widths in a polar coronal hole and nearby regions are obtained from the spectroscopic observations carried out on 1998 November 3 at the Norikura Solar Observatory, Japan. The coronal red line [Fe x]  $\lambda 6374$  that is prominent at coronal hole temperatures is used for the study. The coronal images in Fe IX and Fe x 171 Å and Fe XII 195 Å from the Extreme-Ultraviolet Imaging Telescope (EIT) on the *Solar and Heliospheric Observatory* (*SOHO*) are used to get the temperature map of the corona at the time of observation. Combining both, we have obtained the nonthermal velocities in the region without the usual assumption of a uniform ion temperature. Several plume structures are identified within the coronal hole, and it is found that line widths are smaller in plumes than in the interplume regions, which is also reported from recent *SOHO* observations. The line-of-sight Doppler velocities in the coronal hole are larger than those in the quiet region, probably because of the excess outflow in the coronal hole. A rough negative correlation between intensity and Doppler velocity, similar to that between intensity and line width, is observed in the coronal hole. The typical nonthermal velocity in coronal holes is  $24 \text{ km s}^{-1}$  while that in quiet regions is  $15 \text{ km s}^{-1}$ . The enhanced nonthermal velocity in the coronal hole is suggestive of the important role of the nonthermal broadening mechanism in the acceleration of fast solar wind. Also, the nonthermal velocities are larger (up to 27%) at the interplume regions as compared to plumes. The findings generally support the prevailing view that the interplume regions are the source regions of the fast solar wind.

*Subject headings:* Sun: corona — Sun: UV radiation — radiation mechanisms: nonthermal

### 1. INTRODUCTION

Coronal holes are open magnetic field regions, generally seen at polar regions of the Sun with reduced emission. Coronal holes are important because they are the source regions of the high-speed solar wind (Krieger, Timothy, & Roelof 1973). The mechanism that provides additional momentum to high-speed solar wind remains unknown, and its discovery is one of the fundamental aims of the *Solar and Heliospheric Observatory* (*SOHO*) mission (Domingo, Fleck, & Poland 1995). The possible source is believed to be MHD waves powered by photospheric motions (Ofman et al. 1997). Also, the presence of Alfvén waves has been detected in the solar wind (Smith et al. 1995). The plumes are the fine structures in coronal holes that subtend roughly  $2^\circ$  at the Sun center. They are the familiar raylike structures seen in polar regions in eclipse photographs (Newkirk & Harvey 1968; Fisher & Guhathakurtha 1995). Several decades before these studies, van de Hulst did some pioneering work on plumes (see Wilhelm et al. 1998). Very recently they have been shown to be the extensions of the chromospheric network into the coronal holes rooted at the network cell boundaries (DeForest et al. 1997; Hassler et al. 1999). There has been a recent debate concerning the origin of the fast solar wind, specifically whether it emanates from plumes or interplumes (Ahmad & Withbroe 1977; Hassler et al. 1997).

There has been renewed interest in the fine structures of the coronal holes in recent times, mainly because of the availability of the high-resolution *SOHO* data. The plumes have been known to show changes in small spatial ( $\approx 5''$ )

and temporal ( $\approx$  a few minutes) scales but remain static in large scales (Withbroe 1983; Karovska, Blundell, & Habbal 1994; DeForest et al. 1997; DeForest & Gurman 1998). Signatures of quasi-periodic compressional waves with periods of 10–15 minutes have been reported by Ofman, Nakariakov, & DeForest (1999). Various authors have reported that the emission-line widths in plumes are smaller than in the interplume regions (Hassler et al. 1997; Noci et al. 1997; Wilhelm et al. 1998). The possible explanations of this finding can cause important conclusions in the above debate. One possibility is that plumes are cooler than interplumes. Another possibility is that temperatures in the plume-interplume regions are the same, but there is an enhanced nonthermal broadening in interplume regions due to waves or turbulence (see Hassler et al. 1997). The most recent studies, however, suggest that the origin of the fast solar wind is more likely at the interplumes. According to Wilhelm et al. (1998), the narrower line width in plumes than in interplume regions, the lack of any significant motion in plumes, and the high line-of-sight velocity found in dark regions above the coronal hole all seem to point to the suitability of conditions in the interplume regions for a strong acceleration of the solar wind.

Spectroscopic observations give information about the physical state of the corona and also provide constraints on theories of coronal heating and solar wind acceleration. The line-of-sight Doppler velocities obtained from such observations now point out the existence of a dynamic corona (Chandrasekhar et al. 1991; Raju et al. 1993; Brekke et al. 1997). Another important quantity is the nonthermal velocity, which is thought to be an indicator of the coronal heating mechanism (Harra-Murnion et al. 1999). Transition-region observations have shown that nonthermal velocities increase with increasing temperature according to  $V_{nt} \propto T_e^{0.25}$  for  $\log T_e < 5.8$ , which is predicted

<sup>1</sup> National Astronomical Observatory of Japan, 2-21-1, Ohsawa, Mitaka, Tokyo, 181, Japan.

<sup>2</sup> Indian Institute of Astrophysics, Koramangala, Bangalore, 560-034, India.

from an Alfvén or acoustic wave propagating without dissipation (Mariska, Feldman, & Doschek 1978). However, at coronal temperatures the relationship is not well understood. It has been found that  $V_{nt}$  decreases with  $T_e$  in the range  $\log T_e = 5.8\text{--}6.4$ , while an increasing trend is observed above this range (Tsubaki 1975; Cheng, Doschek, & Feldman 1979; Hara & Ichimoto 1999; Harra-Murnion et al. 1999). The cause of nonthermal broadening, however, is difficult to differentiate (Hassler et al. 1997). Hara & Ichimoto (1999) examine this problem in active regions and find marginal evidence of Alfvén wave components in the nonthermal broadening. The observed nonthermal velocities in the corona are in the range of  $10\text{--}100\text{ km s}^{-1}$  (Acton et al. 1981; Saba & Strong 1991; Sterling 1997). This includes the possible variations in coronal regions. For instance, Dere & Mason (1993) have observed higher values of nonthermal velocity in active regions than in quiet regions.

In the present paper we study the physical conditions in the polar regions of the corona, which includes both open- and closed-field regions. The differences in properties of both regions as well as the differences between plumes and interplume regions are examined. We have used the ground-based coronal spectroscopic data from Norikura and the space-based *SOHO*/Extreme-Ultraviolet Imaging Telescope (EIT) images. An important advantage of our analysis is that we do not assume a constant ion temperature. We believe the study has significance in the above debate and also in various aspects of current coronal physics.

## 2. DATA AND ANALYSIS

The coronal red line [Fe x]  $\lambda 6374$  shows a peak in emissivity at an ion temperature of  $10^6\text{ K}$ , which is the typical coronal hole temperature and hence well suited for coronal hole study. Spectroscopic observations were made on the north polar region on 1998 November 3, using the 25 cm Norikura Coronagraph and Spectrograph at the National Astronomical Observatory of Japan. A  $512 \times 512$  pixel CCD was used as the detector. The details of the instrument are described in Ichimoto et al. (1995) and Singh et al. (1999). The spectrograph slit, which corresponds to  $549'' \times 5''$ , was placed parallel to the solar limb and raster scans were made at 100 positions with steps of  $4''$ . The exposure time used was 40 s. The slit was later moved to a different coronal position, and the scans were repeated. Altogether, five such sets were obtained with some overlap in azimuth. The total position angle coverage was about  $60^\circ$  from the north pole toward the east. The total timespan of the observation was 6.3 hr. The spatial resolution of the data along the slit is  $2''$ , and the spectral resolution is  $0.12\text{ \AA}$ .

The spectra were flat-fielded, and a  $2 \times 2$  pixel averaging was done to improve the signal-to-noise ratio (S/N). Practically no emission was detected beyond  $160''$ , which is expected from a coronal hole region. The coronal redline profiles, in general, were found to be fitted well with single Gaussians. A simulation of the Gaussian fitting program was carried out on synthetic line profiles to estimate the effect of the S/N on fitting errors. It was found that the fitting errors strongly depend on the S/N, and when  $S/N = 10$ , the estimated errors are 5% in intensity,  $1\text{ km s}^{-1}$  in velocity, and  $0.06\text{ \AA}$  in width. We have only considered line profiles with an S/N around 10 and above, which has severely restricted the scope of analysis to the innermost corona.

There are some difficulties in obtaining the absolute velocities in the corona owing to the differences in the wavelengths between the photospheric lines and the laboratory lines (Hassler et al. 1999). To avoid the confusion, the zero point in the velocity is arbitrarily put equal to the prevailing velocities in the corona. Therefore, the Doppler velocities in the present analysis are the relative velocities with respect to the coronal rest frame.

A computer program was used to obtain the line intensities, Doppler velocities, and widths through Gaussian fitting and to combine the results to form a heliogram. Later, the heliograms of individual sets were combined to form a single heliogram, making use of the positional information of the individual observational sets as well as taking care of the azimuthal overlap.

*SOHO*/EIT images in  $171\text{ \AA}$  and  $195\text{ \AA}$  for the time of observation were obtained from Web pages. The pixel resolution of the *SOHO* images is  $2''.6$  (Moses et al. 1997). The temperature map was obtained through line-intensity ratios, using the standard EIT analysis package. A finer alignment between the *SOHO* image and the Norikura intensity heliogram was obtained through an image cross-correlation program. The nonthermal velocities are then obtained from the aligned temperature map and the line width heliogram according to

$$\Delta\lambda^2 = 4 \ln 2 \left( \frac{\lambda}{c} \right)^2 \left( \frac{2kT_i}{M_i} + \xi^2 \right), \quad (1)$$

where  $\Delta\lambda$  is the line width,  $\xi$  is the nonthermal velocity, and  $M_i$  is the mass of the ion.

## 3. RESULTS AND DISCUSSIONS

The heliograms of line intensity are shown in Figure 1. This can be compared with the contrast-enhanced image of  $171\text{ \AA}$  during the time of observation shown in Figure 2. The heliogram covers the northern coronal hole and a quiet region lying just outside. The quiet region contains a loop system and parts of a streamer structure. A few plume structures can be seen at the coronal hole and its boundary.

The temperature map obtained from the EIT images is shown in Figure 3. Zhang, White, & Kundu (1999) in a recent paper discuss the need of considering the two-temperature coronal model from the EIT observations. The temperature map based on  $171\text{ \AA}$  and  $195\text{ \AA}$  images is expected to be appropriate for the present case because (1)

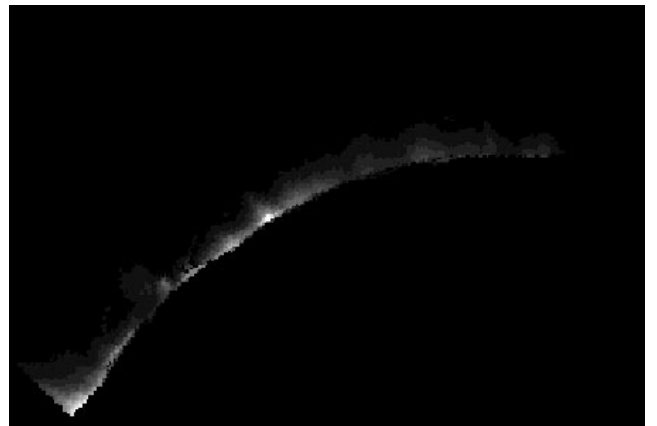


FIG. 1.—Heliogram of the coronal redline intensity

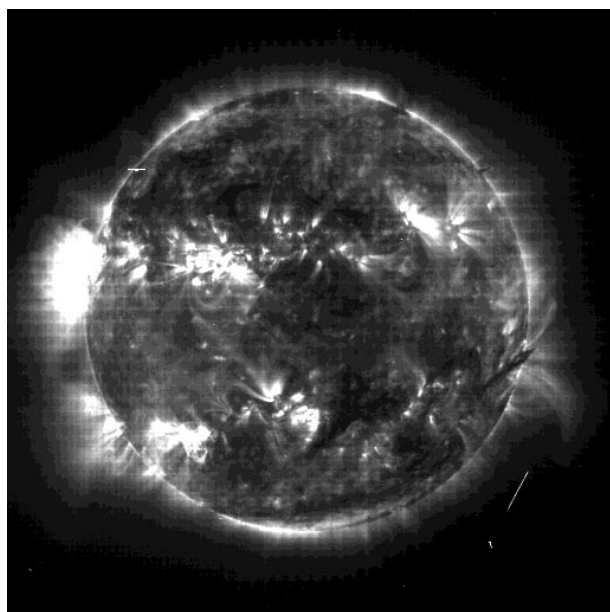


FIG. 2.—Contrast-enhanced *SOHO*/EIT image in 171 Å

we use an emission line prominent at low-coronal temperature ( $\approx 1$  MK), and (2) the regions of interest are a coronal hole and nearby quiet regions.

### 3.1. Histogram Distributions

The histograms of Doppler velocity, line width, and the nonthermal velocity are shown in Figure 4. In the figure the dotted line represents the coronal hole, and the solid line represents the region outside. It can be seen that the histogram distributions show prominent differences between the two regions. The majority of the line-of-sight velocities are in the range of  $-10$  to  $4$   $\text{km s}^{-1}$ , and the magnitudes of the velocities are higher in the coronal hole. It would be incorrect to interpret the line-of-sight velocities as inflow or

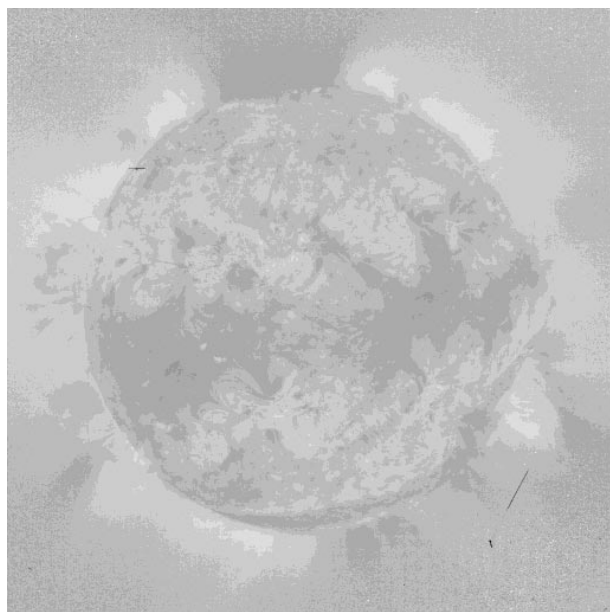


FIG. 3.—Temperature map obtained from the EIT images

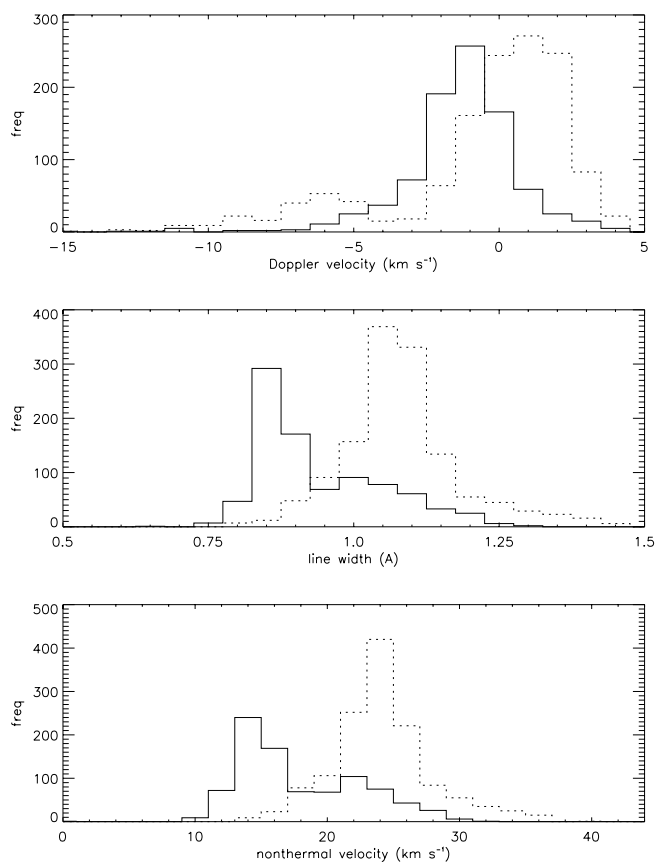


FIG. 4.—Histograms of Doppler velocity (*top panel*), emission-line width (*middle panel*), and nonthermal velocity (*bottom panel*). The dotted line represents the coronal hole, and the solid line represents the quiet region outside.

outflow in a limb observation like ours because we do not have enough information on the geometry of the structures. However, simultaneous disk and limb observations show excess outflow in coronal holes as compared to quiet regions (Rottman, Orrall, & Klimchuk 1981; Dere et al. 1989; Wilhelm et al. 1998). So it is quite probable that the enhanced velocities noted in the coronal hole may be due to the excess outflow.

The histogram distribution of line widths shows that the typical line width in the quiet region is  $0.85$  Å. This is consistent with the earlier observations of the coronal redline widths (Hara & Ichimoto 1999; Singh et al. 1999). We also note that the line widths in coronal holes are about 15% higher than in the quiet regions. The histogram distribution of the nonthermal velocities is somewhat similar to the width distribution. We discuss this point in later sections.

### 3.2. Spatial Variations

The azimuthal variations of various physical quantities in the corona at the radial point  $1.04 R_{\odot}$  are plotted in Figure 5. The typical radial variations in the coronal hole and quiet regions are shown in Figure 6, while that in the plume-interplume regions are shown in Figure 7.

#### 3.2.1. Intensity and Line Width

A general anticorrelation between the intensity and the line width in the coronal hole region can be noted in Figure 5. This is due to the narrower line width in the plumes than in the interplume regions, which is the well-known result

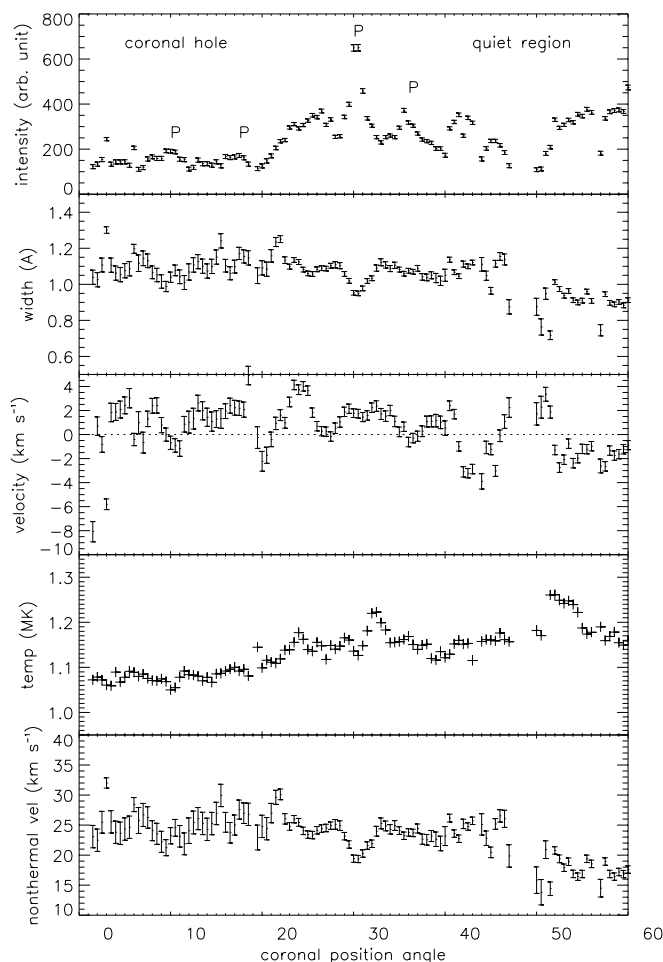


FIG. 5.—Azimuthal variation of various physical quantities in the corona at a radial point  $1.04 R_{\odot}$ . The x-axis represents the coronal position angles from the north pole (zero) toward the east. Prominent plumes are marked as “P.”

from *SOHO* (Hassler et al. 1997; Noci et al. 1997; Wilhelm et al. 1998). It can be seen that the drop in width is proportional to the brightness of the plume. The maximum drop in the line width is up to 18%.

There is a plumelike brightening seen at the pole, albeit with large line widths and Doppler velocities. The detailed examination of the line profiles in this region shows some evidence of multiple components that needs further study. Wilhelm et al. (2000) also find signatures of multi-Gaussian components in the coronal hole line profiles.

### 3.2.2. Doppler Velocity

It may be seen from Figure 5 that there is also an anti-correlation between the line intensity and the Doppler velocity. As discussed earlier, the line-of-sight Doppler velocity is difficult to interpret because of the uncertain projection effects of the coronal structures. However, it is clear that velocities are different in different coronal structures. A distinct change occurs from the interplume to the plume regions; velocities tend to go blueward or approach zero at the center of the plume. However, the radial variations in the coronal hole and quiet region, as well as in the plume and interplume regions shown in Figures 6 and 7, do not show appreciable differences.

There have been only a few reports on the Doppler velocities in coronal holes, and hence, unlike the emission-

line widths, the nature of the Doppler velocities is still unclear. However, the available reports indicate that the plumes have low or no bulk velocities (Wang 1994; Wilhelm et al. 1998; Hassler et al. 1999). The negative correlation between the intensity and Doppler velocity, similar to that between the intensity and line width, seen in Figure 5, agrees well with the above reports.

### 3.2.3. Temperature

The temperature in the coronal hole region is about 1.08 MK and shows a downward trend with coronal height, while in quiet regions the temperature is around 1.2 MK with a clear upward trend. This agrees with the well-known fact that the temperature in the coronal hole is less than that in closed-field regions. The radial variation of temperature in the coronal hole (Fig. 6) supports the view that the available energy is expended in the solar wind acceleration. The analysis, however, brings out an important point; the assumption of a uniform ion temperature, usually employed to obtain the nonthermal velocities, is not well justified.

The azimuthal variation of the temperature shows that it is slightly reduced in the middle of some of the plumes. This is only marginal and at most up to 10% for the brightest plume. Although we do not have the actual error limits on temperature, it can be expected to be of the order of a few percent (Wilhelm et al. 1998), and the temperature difference in the plume-interplume regions is likely to be real. We also find that the radial variations show an increase of temperature with coronal height in both plumes and interplume regions. These results are in variance with some of the recent findings. For instance, Wilhelm et al. (1998) report a significantly (up to 30%) higher temperature for interplume regions. Young, Klimchuk, & Mason (1999) find that the temperature rises with height in the plume background but find no evidence of rising temperature in plumes. We believe that the question of spatial variation of temperature in plume-interplume regions needs to be further examined.

### 3.2.4. Nonthermal Velocity

The nonthermal velocities show clear differences in the coronal hole and quiet regions. In the coronal hole region nonthermal velocities are around  $24 \text{ km s}^{-1}$ , while in the regions outside they are around  $15 \text{ km s}^{-1}$ . From the discussions in the previous section, we conclude that the difference in line widths in the open- and closed-field corona mainly due to the differences in the nonthermal velocity; temperature plays only a secondary role. The radial variations of nonthermal velocity show an increasing trend in the coronal hole, while a decreasing trend is observed in quiet regions. This agrees with the findings of Banerjee et al. (1998), based on *SOHO/SUMER* measurements and the assumption of a uniform ion temperature, where they have reported that the nonthermal velocities increase from  $27 \text{ km s}^{-1}$  at  $27''$  above the limb to  $46 \text{ km s}^{-1}$  at  $250''$ . Following them, the energy flux density due to Alfvén waves, calculated according to

$$F = \sqrt{\frac{\rho}{4\pi}} \langle \delta v^2 \rangle B, \quad (2)$$

where  $\rho$  is the plasma mass density,  $\langle \delta v^2 \rangle$  is the mean square velocity, and  $B$  is the magnetic field strength, is  $4.6 \times 10^7 \text{ ergs cm}^{-2} \text{ s}^{-1}$  for  $B = 10 \text{ G}$  at  $1.06 R_{\odot}$ . This is comparable to the energy requirements of solar wind accel-

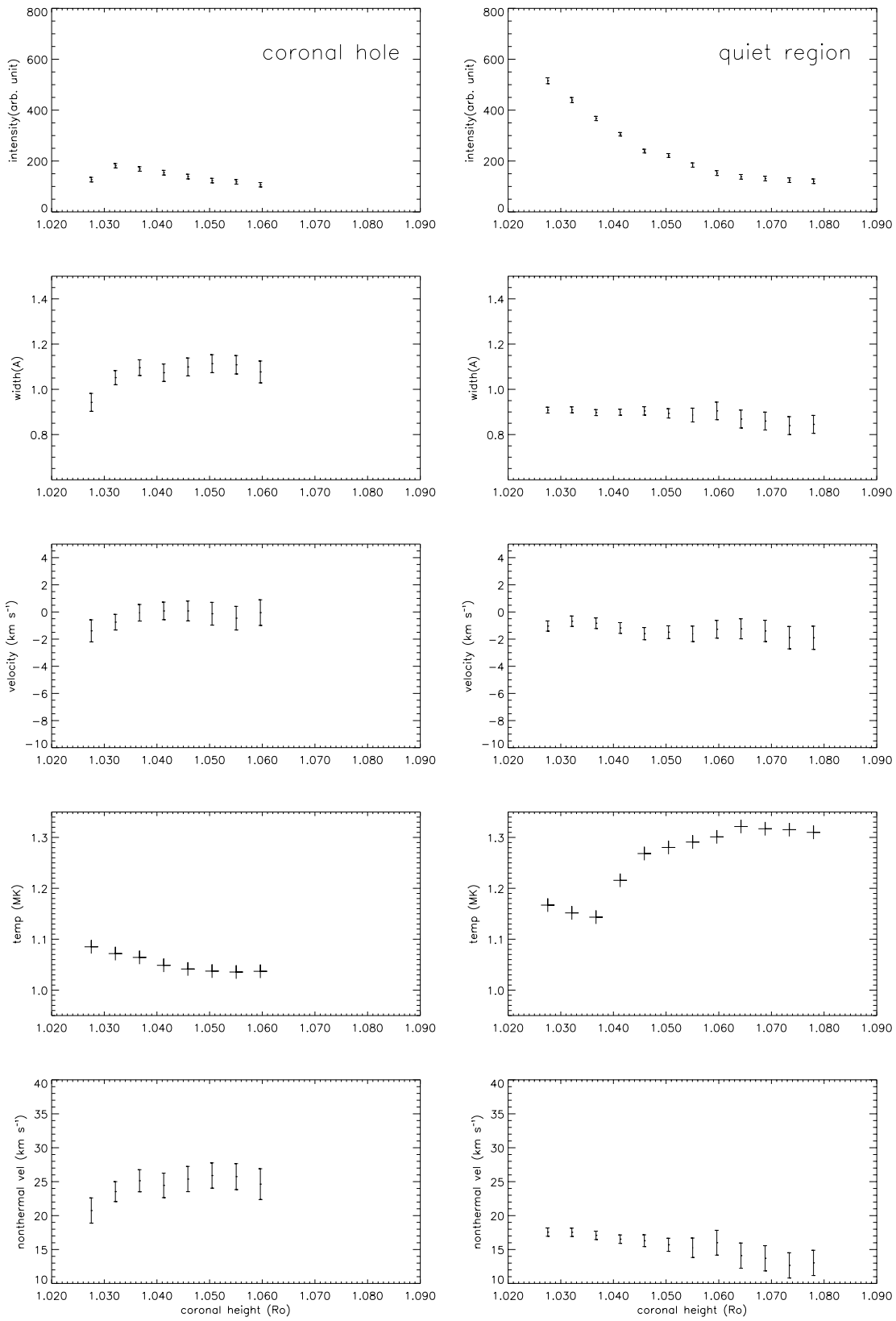


FIG. 6.—Typical radial variations of various physical quantities in the coronal hole and quiet regions

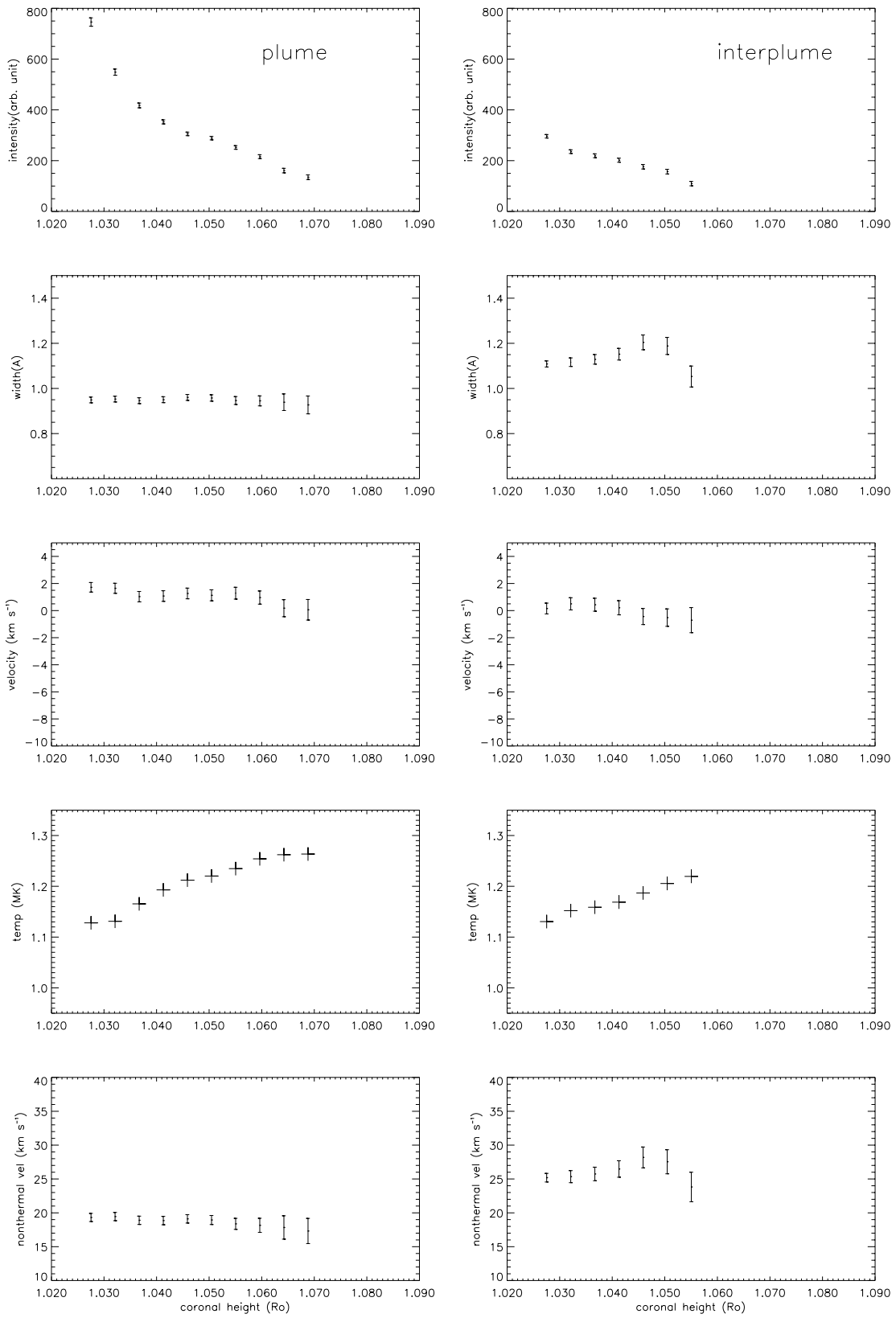


FIG. 7.—Typical radial variations of various physical quantities in the plume and interplume regions

eration (Withbroe & Noyes 1977). Also it can be seen that in the temperature range  $\log T_e = 6.02\text{--}6.12$ ,  $V_{nt}$  has an inverse relationship with  $T_e$ , and this agrees with the earlier findings (Tsubaki 1975; Cheng et al. 1979; Hara & Ichimoto 1999; Harra-Murnion et al. 1999).

The nonthermal velocities show significant differences in plume-interplume regions. In the brightest plume the typical nonthermal velocity is  $19 \text{ km s}^{-1}$ , while in the nearby interplume region it is  $26 \text{ km s}^{-1}$ . However, given the uncertainties in the nonthermal velocities, the radial variations (Fig. 7) remain uncertain. The excess nonthermal broadening in coronal hole regions is likely due to the enhanced dissipation of wave energy in the region, which could be the mechanism of acceleration of the fast solar wind. Similar arguments suggest that interplume regions are the likely source of acceleration sites.

#### 4. CONCLUSIONS

The physical conditions in a polar coronal hole and nearby regions are obtained from ground-based spectroscopic observations from the Norikura and space-based *SOHO* images. The distribution of emission-line intensity, Doppler velocity, line width, temperature, and nonthermal velocities in the inner coronal regions are obtained. The histogram distributions of Doppler velocity, line width, and the nonthermal velocity show prominent differences between the coronal hole and the quiet region. The peak of line width in the coronal hole is  $1.05 \text{ \AA}$  while that in quiet regions is  $0.8 \text{ \AA}$ . A negative correlation between intensity and line width, with smaller widths in plumes than in inter-

plume regions, is seen. We also find a negative correlation between intensity and line-of-sight Doppler velocities in the coronal hole region. This is because the velocities are different in different coronal structures. The Doppler velocities in the coronal rest frame are in the range of  $-10$  to  $4 \text{ km s}^{-1}$ , and the magnitude of the velocities is higher in the coronal hole, which is expected because of the excess outflow in the coronal hole. The temperature map obtained from the *SOHO*/EIT images shows that the temperature in the open-field regions is about  $1.08 \text{ MK}$  and shows a downward fall with height, while in quiet regions the temperature is about  $1.2 \text{ MK}$  with a clear upward trend. This also implies that the assumption of a uniform ion temperature, usually employed to obtain the nonthermal velocities, is incorrect. The typical nonthermal velocity in the coronal hole region is found to be  $24 \text{ km s}^{-1}$  while that in closed-field regions is about  $15 \text{ km s}^{-1}$ . The coronal height dependence of nonthermal velocities is opposite to that of the temperature. As regarding the plume-interplume region difference, we find that the difference in temperature is marginal (up to 10%) while the difference in nonthermal velocities is significant (up to 27%).

This work is partially funded by the Japan Society for the Promotion of Science (JSPS) Invitation Fellowship Program (award L99512). We thank the *SOHO*/EIT principal investigator and the *SOHO*/EIT consortium for the easy availability of the data. One of the authors (K. P. R.) acknowledges the help of the NAOJ staff.

#### REFERENCES

- Acton, L., et al. 1981, *ApJ*, 244, L137  
 Ahmad, I. A., & Withbroe, G. L. 1977, *Sol. Phys.*, 53, 397  
 Banerjee, D., Teriaca, L., Doyle, J. G., & Wilhelm, K. 1998, *A&A*, 339, 208  
 Brekke, P., Kjeldseth-Moe, O., Brynildsen, N., Maltby, P., Haugan, S. V. H., Harrison, R. A., Thompson, W. T., & Pike, C. D. 1997, *Sol. Phys.*, 170, 163  
 Chandrasekhar, T., Ashok, N. M., Desai, J. N., & Pasachoff, J. M. 1991, *Sol. Phys.*, 131, 25  
 Cheng, C. C., Doschek, G. A., & Feldman, U. 1979, *ApJ*, 227, 1037  
 DeForest, C. E., & Gurman, J. B. 1998, *ApJ*, 501, L217  
 DeForest, C. E., Hoeksema, J. T., Gurman, J. B., Thompson, B. J., Plunkett, S. P., Howard, R., Harrison, R. C., & Hassler, D. M. 1997, *Sol. Phys.*, 175, 393  
 Dere, K. P., Bartoe, J.-D. F., Brueckner, G. E., & Recely, F. 1989, *ApJ*, 345, L95  
 Dere, K. P., & Mason, H. E. 1993, *Sol. Phys.*, 144, 217  
 Domingo, V., Fleck, B., & Poland, A. I. 1995, *Sol. Phys.*, 162, 1  
 Fisher, R. R., & Guhathakurtha, M. 1995, *ApJ*, 447, L139  
 Hara, H., & Ichimoto, K. 1999, *ApJ*, 513, 969  
 Harra-Murnion, L. K., Matthews, S. A., Hara, H., & Ichimoto, K. 1999, *A&A*, 345, 1011  
 Hassler, D. M., Dammasch, I. E., Lemaire, P., Brekke, P., Curdt, W., Mason, H. E., Vial, J.-C., & Wilhelm, K. 1999, *Science*, 283, 810  
 Hassler, D. M., Wilhelm, K., Lemaire, P., & Schuhle, U. 1997, *Sol. Phys.*, 175, 375  
 Ichimoto, K., Hara, H., Takeda, A., Kumagai, K., Sakurai, T., Shimizu, T., & Hudson, H. S. 1995, *ApJ*, 445, 978  
 Karovska, M., Blundell, S. F., & Habbal, S. R. 1994, *ApJ*, 428, 854  
 Krieger, A. S., Timothy, A. F., & Roelof, E. C. 1973, *Sol. Phys.*, 29, 505  
 Mariska, J. T., Feldman, U., & Doschek, G. A. 1978, *ApJ*, 226, 698  
 Moses, D. et al. 1997, *Sol. Phys.*, 175, 571  
 Newkirk, G., Jr., & Harvey, J. 1968, *Sol. Phys.*, 3, 321  
 Noci, G., et al. 1997, *Adv. Space Res.*, 20, 2219  
 Ofman, L., Nakariakov, V. M., & DeForest, C. E. 1999, *ApJ*, 514, 441  
 Ofman, L., Romoli, M., Poletto, G., Noci, G., & Kohl, J. L. 1997, *ApJ*, 491, L111  
 Raju, K. P., Desai, J. N., Chandrasekhar, T., & Ashok, N. M. 1993, *MNRAS*, 263, 789  
 Rottman, G. J., Orrall, F. Q., & Klimchuk, J. A. 1981, *ApJ*, 247, L135  
 Saba, J. L. R., & Strong, K. T. 1991, *ApJ*, 375, 789  
 Singh, J., Ichimoto, K., Imai, H., Sakurai, T., & Takeda, A. 1999, *PASJ*, 51, 269  
 Smith, E. J., Balogh, A., Neugebauer, M., & McComas, D. 1995, *Geophys. Res. Lett.*, 22, 3381  
 Sterling, A. C. 1997, *ApJ*, 478, 807  
 Tsubaki, T. 1975, *Sol. Phys.*, 43, 147  
 Wang, Y.-M. 1994, *ApJ*, 435, L153  
 Wilhelm, K., Dammasch, I. E., Marsch, E., & Hassler, D. M. 2000, *A&A*, 353, 749  
 Wilhelm, K., Marsch, E., Dwivedi, B. N., Hassler, D. M., Lemaire, P., Gabriel, A. H., & Huber, C. E. M. 1998, *ApJ*, 500, 1023  
 Withbroe, G. L. 1983, *Sol. Phys.*, 89, 77  
 Withbroe, G. L., & Noyes, R. W. 1977, *ARA&A*, 15, 363  
 Young, P. R., Klimchuk, J. A., & Mason, H. E. 1999, *A&A*, 350, 286  
 Zhang, J., White, S. M., & Kundu, M. R. 1999, *ApJ*, 527, 977